

Article

Hydrogen Evolution Catalysis by a Sparsely Substituted Cobalt Chlorin

Andrew G. Maher, Guillaume Passard, Dilek Kiper Dogutan, Robert L. Halbach, Bryce L. Anderson, Christopher J. Gagliardi, Masahiko Taniguchi, Jonathan Sidney Lindsey, and Daniel G. Nocera

ACS Catal., **Just Accepted Manuscript** • DOI: 10.1021/acscatal.7b00969 • Publication Date (Web): 10 Apr 2017

Downloaded from <http://pubs.acs.org> on April 10, 2017

Just Accepted

“Just Accepted” manuscripts have been peer-reviewed and accepted for publication. They are posted online prior to technical editing, formatting for publication and author proofing. The American Chemical Society provides “Just Accepted” as a free service to the research community to expedite the dissemination of scientific material as soon as possible after acceptance. “Just Accepted” manuscripts appear in full in PDF format accompanied by an HTML abstract. “Just Accepted” manuscripts have been fully peer reviewed, but should not be considered the official version of record. They are accessible to all readers and citable by the Digital Object Identifier (DOI®). “Just Accepted” is an optional service offered to authors. Therefore, the “Just Accepted” Web site may not include all articles that will be published in the journal. After a manuscript is technically edited and formatted, it will be removed from the “Just Accepted” Web site and published as an ASAP article. Note that technical editing may introduce minor changes to the manuscript text and/or graphics which could affect content, and all legal disclaimers and ethical guidelines that apply to the journal pertain. ACS cannot be held responsible for errors or consequences arising from the use of information contained in these “Just Accepted” manuscripts.

Hydrogen Evolution Catalysis by a Sparsely Substituted Cobalt Chlorin

Andrew G. Maher,^{a,‡} Guillaume Passard,^{a,‡} Dilek K. Dogutan,^a Robert L. Halbach,^a Bryce L. Anderson,^a Christopher J. Gagliardi,^a Masahiko Taniguchi,^b Jonathan S. Lindsey^{b,*} and Daniel G. Nocera^{a,*}

^aDepartment of Chemistry and Chemical Biology, Harvard University, 12 Oxford Street, Cambridge, MA 02138

^bDepartment of Chemistry, North Carolina State University, Raleigh, North Carolina 27695

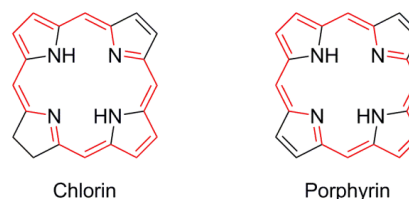
ABSTRACT: A sparsely substituted chlorin macrocycle containing a Co(II) center (**1-Co**) has been synthesized and structurally characterized. The Co(II) atom resides in a square planar coordination environment and induces significant out-of-plane distortion of the chlorin macrocycle. The paramagnetic Co(II) center resides in the macrocycle in a $S = \frac{1}{2}$ spin state, which displays an axial doublet signal ($g_{\perp} \approx 2.3$ and $g_{\parallel} \approx 2.03$) in the X-band EPR spectrum. The open shell d-orbital configuration is manifest in the transient absorption spectrum, which reveals an excited state lifetime of 8.6 ± 0.2 ps for **1-Co**. The Co(II) chlorin exhibits a rich oxidation-reduction chemistry with five reversible one-electron waves (two oxidative processes and three reductive processes) observed in the cyclic voltammogram. The reduction processes of **1-Co** drive hydrogen evolution catalysis. Electrochemical kinetics analysis of HER by **1-Co** in trifluoroacetic acid reveals a hydrogen evolution mechanism that proceeds by an ECEC mechanism. Benchmarking the catalytic activity, **1-Co** exhibits higher HER activity at low overpotentials versus its porphyrin congeners.

Keywords: electrocatalysis, macrocycle, chlorin, cobalt, hydrogen evolution reaction, solar fuels

INTRODUCTION

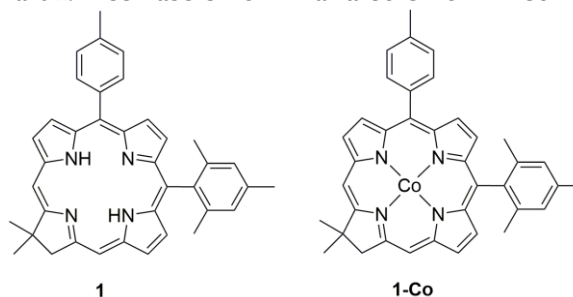
The macrocyclic ring of chlorins is reduced by two electrons and two protons relative to its parent porphyrin structure. The reduction occurs at the β -pyrrolic periphery of the macrocycle and thereby preserves an aromatic 18 π -electron conjugated pathway (Chart 1). Structural data of chlorin macrocycles are consistent with this electronic formulation, as the β, β' -bond external to the 18 π -electron network exhibits a CC distance that is consistent with a more localized π bond.¹ Hence, the macrocyclic core of chlorins is electronically similar but chemically reduced relative to porphyrins. In view of the exceptional catalytic activity of porphyrins in promoting reductive processes such as the hydrogen evolution reaction (HER) and the oxygen evolution reaction (ORR),² chlorins presented an interesting new class of catalysts for the activation of small molecules of energy consequence. The extensive literature on the redox properties and reaction chemistry of porphyrins²⁻⁵ is contrasted by a limited number of studies on the electrochemistry of nickel^{6,7} and iron^{8,9} chlorins. A cobalt chlorin featuring chlorophyll-like substituents is reported to catalyze the two-electron reduction of dioxygen (O_2) to produce hydrogen peroxide (H_2O_2) chemically at activities higher

Chart 1. π -Electron Networks in Chlorins and Porphyrins



than that observed for cobalt porphyrins,^{10,11} which typically drive ORR to H_2O as opposed to H_2O_2 . The same cobalt chlorin has been reported to produce H_2 photochemically at the potential of the photoproducted $Ru(bpy)_3^+$ reductant.¹² The potential dependence of the HER catalysis of chlorins remains undefined, especially

Chart 2. Free Base Chlorin 1 and Co Chlorin 1-Co



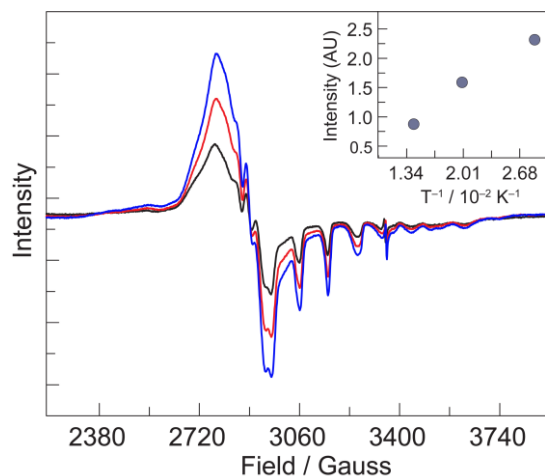


Figure 1. Temperature-dependent EPR spectra (35 K, —; 50 K, —; 70 K, —) of **1-Co**.

with regard to how catalytic activity is influenced by potential.

The study of chlorins has been facilitated by advances in the synthesis of the macrocycle that feature various substituents in specific patterns.¹³ The sparsely substituted chlorin macrocycle **1** (Chart 2) is available from a concise synthesis in appreciable yields¹⁴ to afford material on scales that permit catalysis studies to be undertaken. Moreover, the gem-dimethyl group in the pyrroline ring bestows stability to the chlorin by preventing adventitious dehydrogenation to the porphyrin. We now report the insertion of Co into the chlorin to furnish **1-Co** (Chart 2), which has been structurally characterized. Inasmuch as there are few structurally characterized simple metal chlorin complexes,¹⁵ a comparison of the crystal structure of **1-Co** with that of sparsely substituted chlorin macrocycles furnishes insight to the structural perturbation induced by a centrally chelated metal ion. **1-Co** exhibits a rich redox chemistry, and the various redox species have been correlated to their steady-state and transient electronic spectra. We establish that the redox chemistry of **1-Co** is manifest to an active HER catalysis in the presence of trifluoroacetic acid (TFA). The complex is stable to oxygen, but is unstable in the presence of acid as a promoter of ORR. **1-Co** exhibits higher turnover frequency for HER catalysis at low overpotentials than its porphyrin congeners, likely due to the increased basicity of the chlorin macrocycle.

RESULTS AND DISCUSSION

Preparation and characterization of 1-Co. The free base chlorin **1** is delivered by a *de novo* synthetic route.¹⁴ The *de novo* route builds the chlorin from pyrrolic constituents rather than relying on the more prevalent route wherein a porphyrin is converted to a chlorin.¹⁶ A modified procedure was used to insert Co(II) into the macrocycle.¹⁷ The metalation proceeds quantitatively over 48 h upon treatment of **1** with 82 mol excess Co(OAc)₂ in

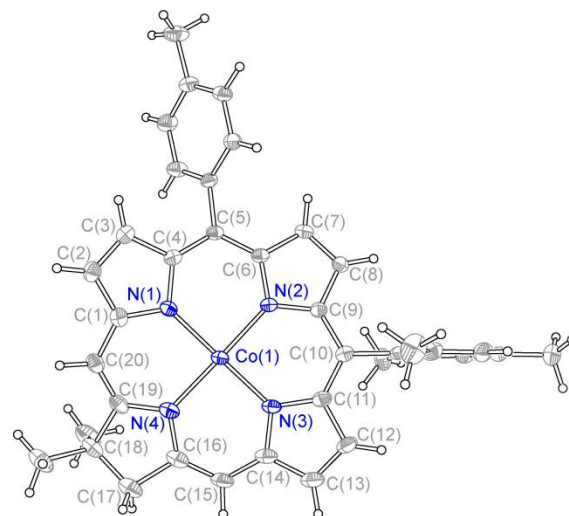


Figure 2. Solid-state structure of **1-Co** with thermal ellipsoids (drawn using SHELX/XP) shown at the 50% probability level. Selected interatomic distances (Å) and angles (deg): $d(\text{Co1-N1}) = 1.9445(17)$, $d(\text{Co1-N2}) = 1.9660(17)$, $d(\text{Co1-N3}) = 1.9465(18)$, $d(\text{Co1-N4}) = 1.9901(18)$, $d(\text{C7-C8}) = 1.356(3)$, $d(\text{C17-C18}) = 1.520(4)$, $\angle(\text{C1-N1-C4}) = 104.66(18)$, $\angle(\text{C6-N2-C9}) = 104.67(17)$, $\angle(\text{C11-N3-C14}) = 104.82(18)$, $\angle(\text{C16-N4-C19}) = 107.27(19)$.

CH₂Cl₂/CH₃OH (4:1) mixtures under anaerobic conditions in a glove box. The metalation of the chlorin is evident by the paramagnetic broadening of the ¹H NMR resonances (Figure S1a), which stand in contrast to the sharp resonances observed in the ¹H NMR spectrum of **1** (Figure S1b), and the FTIR spectrum. For the latter, the N–H stretching vibration at 3343 cm⁻¹ in free base chlorin **1**, which is similar to that for free base porphyrins (3310–3326 cm⁻¹),¹⁸ disappears upon cobalt insertion (Figure S3). On the basis of similar assignments in free base and nickel porphyrin derivatives,¹⁸ two weak bands between 2750 and 3000 cm⁻¹ are assigned to the C–H stretching bands of the meso-carbons, intense vibrations at 1595 and 1620 cm⁻¹ are assigned to C=C stretching vibrations, and bands at 1350 cm⁻¹ are assigned to C–N stretching vibrations. The formulation of **1-Co** has also been confirmed by high resolution LC-MS in the positive ion mode (Figure S4) with $m/z = 605.2211$ (for M⁺, where M = C₃₈H₃₄CoN₄, calcd 605.2115).

The paramagnetic properties of **1-Co**, indicated by the broad peaks in the ¹H NMR spectrum, are verified by the EPR spectrum of the complex (Figure 1). Under anaerobic conditions, **1-Co** exhibits typical EPR signatures for a Co(II) ion in the tetragonal field of the chlorin macrocycle. The X-band EPR spectrum exhibits an axial doublet signal with a quasi-axial g tensor of $g_{\perp} \approx 2.3$ and $g_{\parallel} \approx 2.03$. These g values are consistent with a low spin, S = ½ spin system with the unpaired electron occupying the d_{z²} orbital. Strong and well-resolved ⁵⁹Co hyperfine couplings of 98 G are observed for A_∥, consistent with other Co(II) macrocycles.^{19,20}

Dark green crystals of **1-Co** were obtained by cooling a

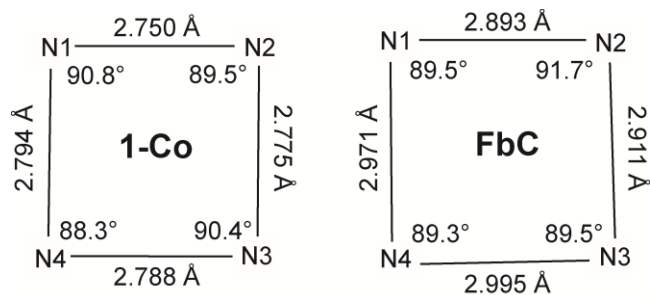


Figure 3. The inner core of sparsely substituted chlorin in the presence and absence of a metal.

saturated solution of **1-Co** in pentane at -20 °C. Figure 2 displays the x-ray crystal structure for which the details of structure determination are listed in Table S1. The central cobalt atom resides in a square planar coordination environment defined by the chlorin macrocycle, which deviates from an ideal planar system. The average Co–N bond distance of the pyrrolic rings is $1.952(3)$ Å whereas the Co–N bond distance of the pyrroline unit is $1.9901(18)$ Å. The mesityl substituent is nearly perpendicular (82°) to the mean plane of the macrocycle whereas the *p*-tolyl substituent is less twisted (51°) (Figure 2).

The chlorin macrocycle of **1-Co** undergoes significant out-of-plane distortion upon metalation, in contrast to the structure of a related free base chlorin,¹ **FbC**, which exhibits a nearly planar macrocycle. The distortions from planarity can be accounted for by the sum of the absolute values of the positive and negative displacements of the nitrogen atoms of the chlorin from a plane (defined by the four nitrogen atoms).¹ The average out-of-plane distortion of **FbC** is 0.044 Å, whereas the average distortion of **1-Co** is 0.261 Å. Table S2 compares the average deviation from planarity to other free base chlorins as well; in all cases **1-Co** is more distorted. Metalation also alters the structural metrics of the pyrroline ring, as shown in Table S3; there is an increase in the C_α – C_β ($C16$ – $C17$) bond distance of the pyrroline ring and a decrease in the C_α – C_β ($C17$ – $C18$) and C_α – C_β ($C18$ – $C19$) bond distances of **1-Co** as compared to **FbC**. The most notable change in the bond angles between **1-Co** and **FbC** is observed at $C17$ and $C18$ where the hybridization changes from sp^2 to sp^3 . The bond angles of $C16$ – $C17$ – $C18$ ($103.13(19)^\circ$) and $C17$ – $C18$ – $C19$ ($100.27(19)^\circ$) in **1-Co** are narrowed by 3.7° and 6.8° , respectively, compared to the corresponding bond angles in **FbC**. Compensation for these narrowed angles ($\sim 10.5^\circ$ in total) in the 5-membered ring occurs by widening of the remaining three angles: $C16$ – $N4$ – $C19$ ($\sim 2.1^\circ$), $N4$ – $C16$ – $C17$ ($\sim 1.5^\circ$), and $C18$ – $C19$ – $N4$ ($\sim 1.7^\circ$). Metalation also leads to a change in the C_α – N – C_α framework bond angles (Table S4) as well as the core shape and core size of the macrocycle (Table S5). As shown in Figure 3, the core size of **1-Co** is contracted relative to the free base species **FbC** and becomes more symmetric upon insertion of Co into the chlorin macrocycle, almost assuming a square as opposed to the more trapezoidal core of **FbC**. Thus whereas metal

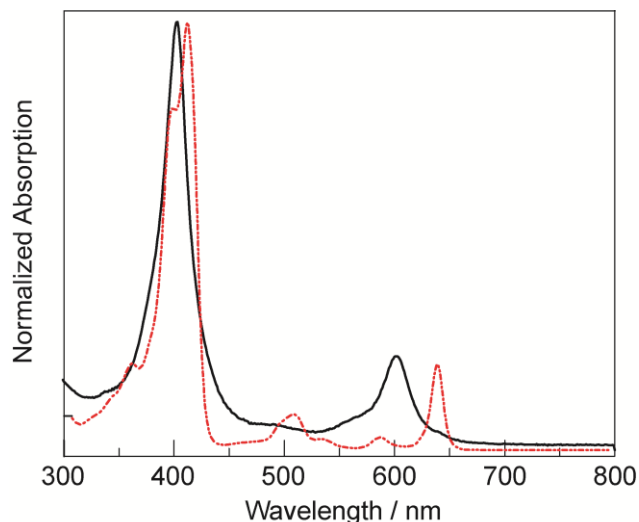


Figure 4. Absorption spectra of **1** (---) and **1-Co** (—) at room temperature in CH_2Cl_2 . The spectra are normalized with respect to the Soret band intensities.

insertion causes the core composed of the four nitrogens to assume a more square-like geometry, there is much greater out-of-plane distortion resulting from the metal insertion.

Another notable structural metric is the bond distance (Table S6) of the pyrrolic C_β – C_β bond $C7$ – $C8$, which is the double bond external to the 18 π -electron conjugated pathway shown in Chart 1. The $C7$ – $C8$ double bond of **1-Co** is $1.356(3)$ Å, which is statistically indistinguishable from the other C_β – C_β bond distances of **1-Co** ($C2$ – $C3 = 1.344(3)$ Å, $C12$ – $C13 = 1.345(3)$ Å) because the differences in bond lengths are not more than three times greater than the estimated standard deviations added in quadrature.²¹ A similar comparison of the $C7$ – $C8$ bond with respect to the other C_β – C_β bonds has also been observed in nickel tetramethylchlorin ($C7$ – $C8 = 1.362$ Å, $C2$ – $C3 = 1.353$ Å, $C12$ – $C13 = 1.351$ Å).¹⁵ These results stand in contrast to the trend seen in the free base **FbC**, in which the $C7$ – $C8$ bond distance of $1.3588(19)$ Å is shorter than the other C_β – C_β distances ($C2$ – $C3 = 1.3704(19)$ Å, $C12$ – $C13 = 1.3680(19)$ Å) to a statistically significant extent. The shortening of the $C7$ – $C8$ bond in the free base chlorin could be a manifestation of the exclusion of that bond from the extended π -electron network in order to avoid an anti-aromatic 20 π -electron count. In this regard, the lack of shortening of the $C7$ – $C8$ bond in the metalated chlorins suggests that the presence of the metal center may lessen the anti-aromaticity of the 20 π -electron network.

The absorption spectra of **1** and **1-Co**, shown in Figure 4, exhibit the signature B(Soret)- and Q-bands common to tetrapyrrole macrocycles as well as the enhanced Q-band intensity in the red region particular to chlorins,²² though the two spectra differ significantly from each other. With respect to the absorption spectrum of **1**, **1-Co** exhibits a ~ 10 nm hypsochromic shift of the B(o,o) Soret band and a ~ 40 nm hypsochromic shift of the $Q_y(o,o)$

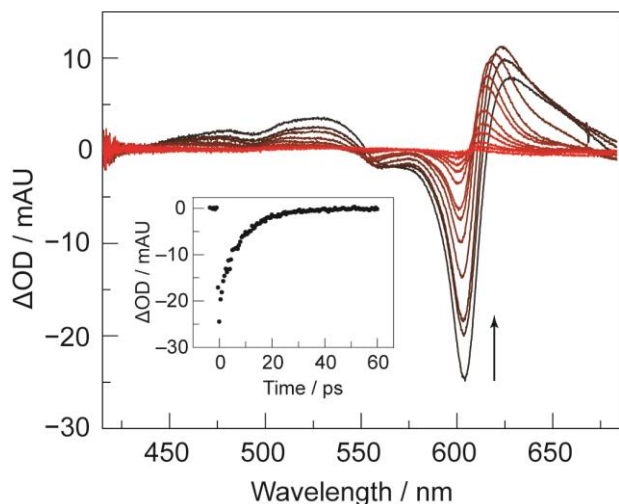


Figure 5. Transient absorption spectra of **1-Co** at room temperature in toluene at time delays ranging from < 1 ps (black) to 60 ps (red) using an excitation wavelength of 400 nm. Inset: single wavelength kinetics trace monitored at 604 nm.

band. The split in the Soret band of **1**, which is common in free base chlorins, is due to the partial resolution of the x - and y -polarized components. The split Soret is not observed for **1-Co**, consistent with reports of coalescence of B_x and B_y bands in other metallochlorins, though the exact nature of the relative positioning of the B_x and B_y bands in chlorins is not yet fully understood.²³⁻²⁵

Transient Absorption Spectroscopy. The excited state of **1-Co** is short-lived as expected for an open shell d -orbital metal ion in a π -aromatic system. In the absence of emission, the excited-state dynamics were examined by picosecond transient absorption (TA) spectroscopy. Figure 5 displays the visible light picosecond TA spectrum of **1-Co** in toluene upon excitation with a 400 nm laser pulse at a variety of time delays between < 1 ps and 60 ps. Samples of **1-Co** are indefinitely stable under TA excitation conditions (Figure S5). The transient difference spectrum shows a prompt broad absorption growth (between 425 nm and 550 nm) and bleaches of the ground state Q bands. Additionally, an absorption band slightly to the red of the intense 604 nm ground state bleach grows in over the first few picoseconds. By 60 ps, the transient spectrum has returned to baseline, indicating that excited **1-Co** completely relaxes back to its electronic ground state during that time interval. A biexponential least-squares fit of the single-wavelength trace at 604 nm (Figure 5 inset) yields time constants of 700 ± 100 fs for the short component decay and 8.6 ± 0.2 ps for the long component decay. A monoexponential fit of the fast growth process at 618 nm yields a time constant of 660 ± 40 fs, which matches the faster component of the biexponential bleach at 604 nm. The faster dynamical process is observable for both 400 nm and 600 nm excitation wavelengths, indicating that it is not due to internal conversion from the ${}^3B(\pi, {}^*\pi)$ excited state to the

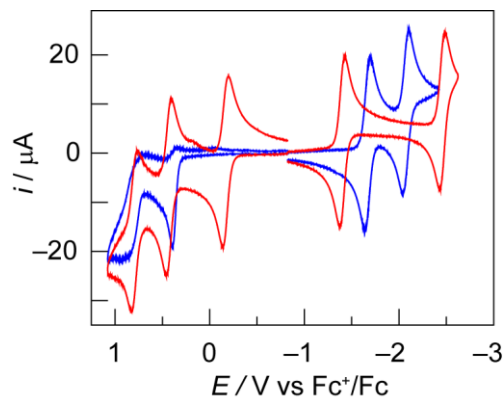


Figure 6. CVs of **1-Co** (—) and **1** (—) (1 mM) in CH_3CN (0.1 M TBAPF₆) at a scan rate of 0.1 V s^{-1} under an Ar atmosphere with a glassy carbon working electrode (3 mm).

${}^2Q(\pi, {}^*\pi)$ state. Rather, the fast component may reflect vibrational cooling, intersystem crossing to either a doublet ${}^2T(\pi, {}^*\pi)$ or quartet ${}^4T(\pi, {}^*\pi)$ excited state, or relaxation to a (d,d) or charge-transfer excited state. The 8.6 ps overall excited-state lifetime of the **1-Co** in toluene is similar to those obtained for other Co(II) tetrapyrrole macrocycles such as porphyrins, which typically have lifetimes shorter than 20 ps, attributable to the formation of a low-lying ligand-to-metal charge-transfer (LMCT) state.^{26,27} The very short lifetime of **1-Co** is in contrast to the free base and Zn chlorin analogs, which have singlet excited state lifetimes of 10.7 ns and 1.6 ns respectively,²³ underscoring the influence of the open-shell cobalt on the electronic structure of the complex.

Oxidation Reduction Chemistry. Chlorins **1** and **1-Co** exhibit a rich redox chemistry. The CVs of **1** and **1-Co**, shown in Figure 6, reveal a number of reductive and oxidative redox processes, all of which are electrochemically reversible in the case of **1-Co**. From the resting state, **1-Co** shows two reduction waves at standard potentials of $E_{1-}^0 = -1.401$ and $E_{2-}^0 = -2.460$ V vs. Fc^+/Fc (Figure 6, red line). The compound also exhibits three oxidation waves centered at $E_{1+}^0 = -0.167$, $E_{2+}^0 = 0.430$ and $E_{3+}^0 = 0.796$ V vs. Fc^+/Fc . A comparison of the CV of **1-Co** to that of **1** (Figure 6, blue line) shows that the two most negative reduction processes and two most positive oxidative processes are largely associated with the redox chemistry of the chlorin. The E_{2+}^0 oxidation process for **1-Co** occurs at a similar potential to the first oxidation of **1** as well as that of other free base and zinc chlorins,²⁸ further supporting the assignment of a ligand-centered oxidation. It is interesting to note that while the E_{2+}^0 and E_{3+}^0 oxidative processes for **1-Co** occur at nearly identical potentials as the two most positive oxidations of **1**, the processes are quasi-reversible for free base **1** but reversible for the metal-containing **1-Co** chlorin. The irreversibility of these oxidation processes in chlorins and isobacteriochlorins has been suggested to stem from oxidative dehydrogenation leading to porphyrin species,^{7,29} but in our case the presence of geminal methyl groups at the 18 position of the macrocycle makes

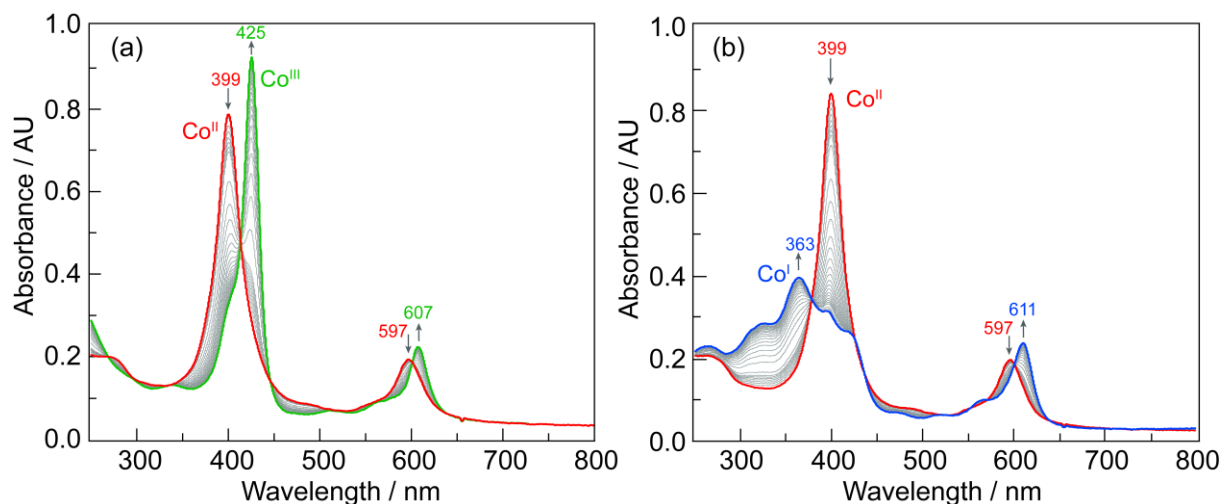


Figure 7. (a) Thin-layer UV-vis spectroelectrochemistry of **1-Co** in CH_3CN and 0.1 M TBAPF₆ in a nitrogen-atmosphere glovebox at room temperature (a) Potential held at 0.04 V vs Fc^+/Fc . The Co(III/II) couple is shown with Co(II) (—) and Co(III) (—). (b) Potential held at -1.51 V vs. Fc^+/Fc . The Co(II/I) couple is shown with Co(II) (—) and the tentatively assigned Co(I) (—).

porphyrin formation unlikely, especially in the absence of strong acid. The reversibility of the oxidations of **1-Co** suggests that replacing the two *N*-pyrrolic protons with a metal center prevents a ligand-based chemical step, such as deprotonation of the *N*-pyrrolic protons upon oxidation. This contention is supported by the observation that the first oxidation of the analogous Zn chlorin complex, **1-Zn**, which occurs at a similar standard potential (0.30 V vs. Fc^+/Fc) to that of **1**, is also reversible.²⁴ Concerning the reductive processes, we note that an overlay of the CVs (Figure 6) reveals that the reductive processes (E_{1-}^0 and E_{2-}^0), in contrast to the two most positive oxidative processes, are perturbed considerably by the presence of the Co ion within the chlorin core, with the first reduction shifting in the positive direction and the second reduction shifting to a more negative potential with respect to **1**. Thus, the reduction processes likely involve molecular orbitals with considerable admixtures of the Co d-orbitals with the chlorin frontier orbitals. For simplicity and the purposes of the work described herein, we will use a metal oxidation state formalism and describe the reductions as Co(II/I) and Co(I/o) processes with the caveat that these reductions have a parentage involving the chlorin macrocycle.

We ascribe the unique CV wave of **1-Co** at $E_{1+}^0 = -0.167$ V to the Co(III/II) redox process. This value for the first oxidation of **1-Co** falls within the range of reported values for the Co(III/II) couple of cobalt porphyrins, though the reduction potential for the Co(III/II) couple of cobalt tetraphenylporphyrin is highly variant (-0.40 to +0.60 V vs Fc^+/Fc) and depends markedly on the solvent and electrolyte used.³⁰ The Co(III/II) couple of **1-Co** was further interrogated using thin-layer UV-vis spectroelectrochemistry by applying an electrochemical potential of 0.04 V vs. Fc^+/Fc . Upon application of the potential, the Soret band at $\lambda_{\text{max}} = 399$

nm bathochromically shifts to $\lambda_{\text{max}} = 425$ nm with a concomitant increase in molar absorption coefficient. The $Q_y(o,o)$ band also undergoes a bathochromic shift, moving 10 nm from 597 nm to 607 nm while maintaining well-anchored isosbestic points (Figure 7a). The shifts of the Soret and Q bands are consistent with spectral changes expected for oxidation of the Co(II) ion to Co(III) within the chlorin macrocycle. In addition, no absorption is observed in the 450-500 nm region of the spectroelectrochemical difference spectrum of Figure 6a; broad growths in this region are observed for π -cations of macrocycles such as porphyrins.^{31,32} Indeed, in the TA (Figure 5), we do see growths in this region, consistent with an LMCT transition. Thus, the absence of absorptions in this region of the difference spectroelectrochemistry provides further support for an oxidation process occurring largely at the metal center. Consistent with the electrochemical reversibility of this redox couple, the spectrum cleanly reverts to that of Co(II) when the potential is held at open circuit.

The reduced form of the Co(II) chlorin was interrogated similarly, by applying an electrochemical potential of -1.51 V vs Fc^+/Fc . Upon application of potential, the Soret band decreases in intensity and splits, with the new bands forming at 363 nm and 421 nm. The $Q_y(o,o)$ band shifts 14 nm to 611 nm (Figure 7b). Such spectral shifts likely correspond to the Co(II/I) redox couple; the shifts are reversible upon returning cleanly back to Co(II) when held at open circuit potential.

The spectral changes observed upon controlled potential electrolysis of **1-Co** at 0.04 V and -1.51 V, especially for the Soret bands, are similar to those observed upon the formation of Co(III) and Co(I) porphyrins, respectively,^{33,34} thus supporting the assignment of Co(III) for the one-electron oxidized chlorin complex and of a formal Co(I) chlorin for the one-electron reduced complex. In particular, the split Soret

band we observe for the Co(I) chlorin has also been observed for Co(I) porphyrins, and in the latter case the origin of the higher energy band has been attributed to a double excited state of charge-transfer character on the basis of magnetic circular dichroism experiments.^{33,35} The similarity between the spectra of the Co(I) chlorin and those reported for Co(I) porphyrins suggests that the first reduction of both species are similar in nature with regard to the site of electron transfer. The first reduction of Co(II) porphyrins has conventionally been assigned as metal-centered because the resulting complexes are diamagnetic.^{36,37} However, in light of recent reports detailing the antiferromagnetic coupling of non-innocent macrocycle ligand radicals to metal centers with odd d-electron counts,³⁸ diamagnetism alone is insufficient to definitively assign whether the nature of the reduction is purely metal-centered, purely ligand centered, or a combination of the two.

Electrocatalysis. With access to **1-Co** on scales approaching 20-100 mg per synthesis, we were able to undertake exploratory studies of **1-Co** as a small molecule reduction catalyst with emphasis on ORR and HER. With regard to the former, the addition of O₂ has no effect on the Co(III/II) (E_{1+}^0) process, which remains fully reversible and unchanged in potential (Figure 8a) during CV cycling. In the presence of both oxygen and acid, however, the catalyst decomposes to a yet unidentified product. This chemical instability is evident by the prompt decrease in the current of the Co(III/II) CV wave upon the addition of 1 mM chloroacetic acid (ClAcOH) to an oxygenated solution of **1-Co**. A catalytic wave is observed to more negative potentials under these conditions, and the current of this wave varies over time. A stable current and reproducible CV is achieved only after 30 min (Figure 8b). Addition of acid results in an increase in catalytic ORR current (Figure 8c). We

attribute this catalysis to the decomposition product of **1-Co**. The decomposition may be reproduced chemically when **1-Co** is exposed to humid air over long periods of time. The CV waves of **1-Co** in air-decomposed samples are negligible (Figure S6a). Notwithstanding, we observed high ORR activity from the decomposed product (Figure S6b) that is very similar to that shown in Figure 8c, as is evident when the traces are overlaid (Figure S6c). We therefore conclude that **1-Co** decomposes in the presence of oxygen *and* acid, most likely due to a slow reaction with oxygen that is accelerated via an acid-catalyzed process. It is this decomposition product that gives rise to the apparent ORR activity of **1-Co**. We note the recent reports of Co chlorins as selective ORR catalysts for H₂O₂ production from O₂; the chlorins are naturally derived and differ structurally from **1-Co**.^{10,11} The generality of the decomposition phenomenon observed herein for **1-Co** is not known across other Co chlorins but warrants investigation.

Whereas the chlorin framework of **1-Co** appears to be unstable in an environment containing both acid *and* oxygen, it is stable in the presence of acid alone with the caveat that acids that are too strong will lead to demetalation of the chlorin. For example, a CV wave ($E_p = -1.3$ V vs Fc^{+/Fc}) appears to potentials positive of the Co(II/I) couple when **1-Co** is titrated with a strong acid such as *p*-toluenesulfonic acid (pTSA, pK_a = 8.6 in CH₃CN),³⁹ as shown in Figure S7. Bulk electrolysis performed at potentials < -1.3 V vs Fc^{+/Fc} confirms demetalation of **1-Co**, as the absorption spectrum of the solution following bulk electrolysis shows the presence of **1** (Figure S8); thin layer chromatography (Figure S9) and HR-MS (Figures S10 and S11) also establish the presence of demetalated chlorin. Conversely, bulk electrolysis of **1-Co** performed in the presence of weaker acids such as ClAcOH (pK_a = 15.3 in CH₃CN)³⁹ and TFA (pK_a = 12.7 in

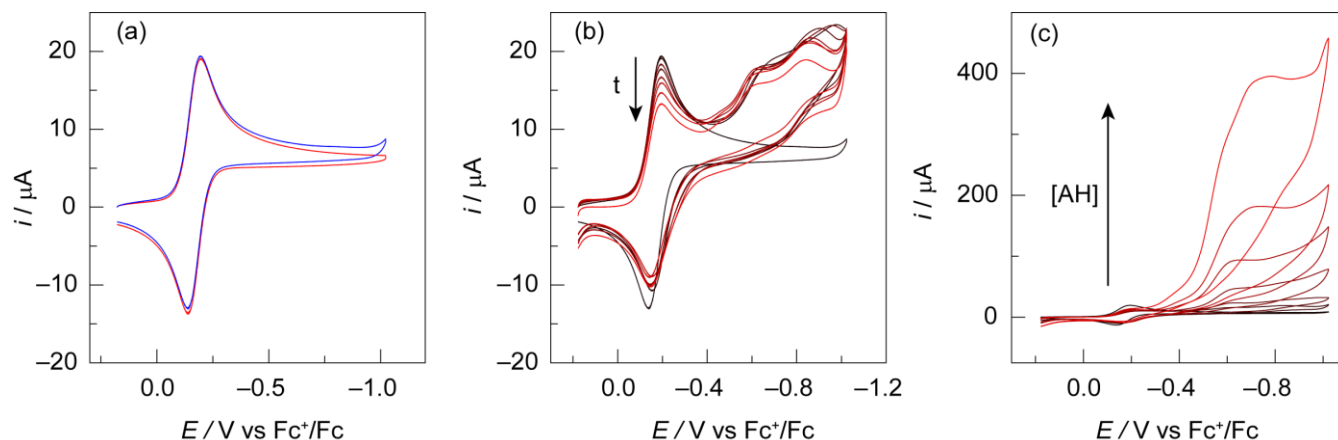


Figure 8. (a) CVs of E_{1+}^0 process of **1-Co** (1 mM) in CH₃CN (0.1 M TBAPF₆) at a scan rate of 0.1 V s⁻¹ with a glassy carbon working electrode (3 mm) under an Ar atmosphere (—) and in a saturated O₂ solution (8.1 mM) (—). (b) CVs of **1-Co** (1 mM) in CH₃CN (0.1 M TBAPF₆) at a scan rate of 0.1 V s⁻¹ with a glassy carbon working electrode (3 mm) in a saturated O₂ solution (8.1 mM) in the presence of 1 mM chloroacetic acid. Evolution with time: from 0 min (—) before the addition of acid until 30 min (—). Around 5 min elapsed between each CV. (c) CVs of **1-Co** (1 mM) in CH₃CN (0.1 M TBAPF₆) at a scan rate of 0.1 V s⁻¹ with a glassy carbon working electrode (3 mm) in a saturated O₂ solution (8.1 mM). Addition of chloroacetic acid: 0 (—), 1, 2, 5, 10, 20 and 50 mM (—).

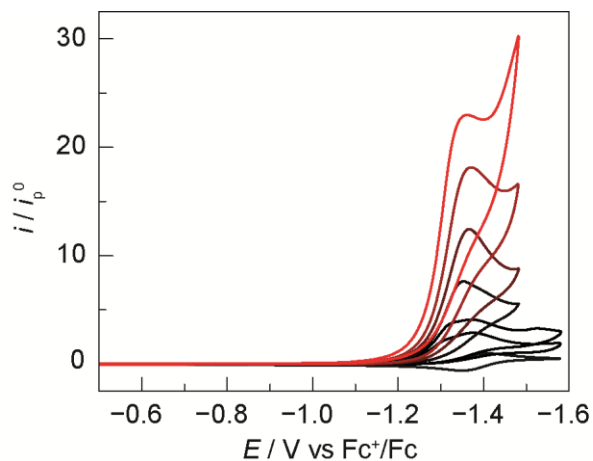
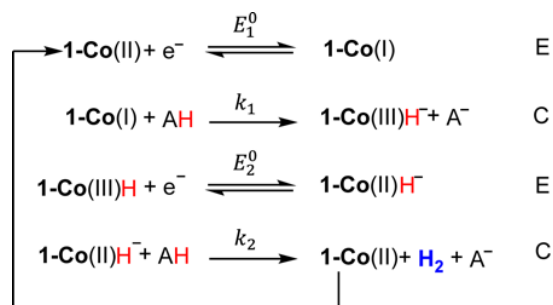


Figure 9. CVs of **1-Co** (1 mM) in CH_3CN (0.1 M TBAPF_6) at a scan rate of 0.1 V s^{-1} under an Ar atmosphere with a glassy carbon working electrode (3 mm). Addition of trifluoroacetic acid: 0 (—), 1, 2, 5, 10, 20, 50 (—) mM.

CH_3CN)³⁹ show no presence of **1** in absorption spectra of bulk-electrolyzed solutions. Accordingly, to avoid complications arising from demetalation, we undertook the study of HER catalysis by **1-Co** under these weaker acid conditions. In considering the choice of the weaker acid, reduced Co tetrapyrrole macrocycles are known to be strong nucleophiles and thus HER reactions may be complicated by competing $\text{S}_{\text{N}}2$ reactions of weak C–X bonds. Such reactivity has been observed for Co porphyrins and cobalamin complexes, which perform catalytic reductive dechlorination of alkyl chlorides.^{40,41} Indeed, the use of ClAcOH as a weak acid in the presence of reduced Co chlorin species showed the presence of chloride formation in competition with HER. Accordingly, studies of HER focused on the use of TFA, which is less prone to nucleophilic attack by the reduced Co chlorin center owing to the presence of stronger C–F vs C–Cl bonds.

Titration of TFA to **1-Co** gives rise to a significant increase in current of the Co(II/I) (E_{1-}^0) wave (Figure 9), indicating catalysis. GC analysis of the headspace following bulk electrolysis in this case showed H_2 evolution (Figure S12), with a faradaic efficiency of 67%. Analysis of the catalytic CV traces in Figure 9 provides insight into the HER mechanism. Specifically, the half-wave potential of the catalytic wave, which is the potential at which the current is at half of its peak height, may be used to determine the sequence of electrochemical (E) and chemical (C) steps in the mechanism (Scheme 1). Possible sequences include ECEC, EECC, and ECCE mechanisms. Beginning with the Co(II) chlorin, an EECC mechanism would require two one-electron reductions prior to a chemical step. As the catalytic wave occurs after one one-electron reduction, near the Co(II/I) reduction potential and well positive of the Co(I/o) potential, an EECC mechanism from the Co(II) chlorin appears unlikely. An irreversible one-electron wave would be observed in the case of an ECCE

Scheme 1. Proposed HER Mechanism for by **1-Co**



mechanism in which the second electron transfer is more difficult than the first.⁴² This is not observed in the CVs (Figure 9), so this case is also ruled out. An ECCE mechanism in which the second electron transfer is easier than the first is equivalent to an EECC mechanism in terms of the dependency of the half-wave potential on the rate constants for proton transfer.⁴² Conceptually, one could view this type of ECCE mechanism from the Co(II) chlorin as equivalent to an EECC mechanism from the Co(III) chlorin. In such an ECCE or EECC case the half-wave potential of the catalytic wave could only be shifted positive of the standard potential of the catalyst by a maximum of $\frac{RT}{F} \ln 2 = 17.6 \text{ mV}$, regardless of the values of the rate constants for electron transfer or proton transfer.^{42,43} For **1-Co**, the half-wave potential is constant and at a potential positive of the standard potential of the Co(II/I) couple by 99 mV, as shown in Figure 10b. The position of the half-wave potential is therefore inconsistent with an ECCE mechanism with Co(II) chlorin as the initial species. Accordingly, HER catalysis by **1-Co** is most consistent with an ECEC mechanism in which sequential electrochemical reduction and chemical steps occur.

The S-shape of the catalytic wave at high acid concentration ($\geq 5 \text{ mM}$) in Figure 9 is consistent with HER limited only by the kinetics of the catalytic reaction as opposed to the diffusion of the substrate (the acid).⁴⁴ Under such conditions, the plateau current provides invaluable mechanistic insight, particularly with regard to the nature of H_2 production. The two consensus mechanisms for H_2 generation are “heterolytic” or “homolytic” reaction pathways where the former involves protonation of a metal hydride (a hetero-coupling event) and the latter involves homolytic dissociation of the two metal hydride bonds.⁴⁵ Costentin, Dridi, and Savéant have shown that these two pathways may be distinguished by analysis of the plateau current and the location of the half-wave potential. In the case of the titration of **1-Co** with TFA, the plateau current is proportional to the square root of the acid concentration (Figure 10a). This observation, in conjunction with the aforementioned observation that the half-wave potential is constant and more positive than the standard potential, is consistent with the prevalence of a heterolytic pathway for H_2 production.⁴⁵

The mechanism for HER by **1-Co** proposed in Scheme 1 reflects a heterolytic pathway that conforms to an ECEC mechanism. In this proposed mechanism, one-electron reduction of the Co(II) species is followed by protonation of Co(I) to deliver a Co(III)H hydride. Subsequent one-electron reduction of Co(III)H to Co(II)H produces an intermediate with increased hydricity, thus driving a second protonation to produce hydrogen and close the catalytic ECEC cycle. We do not see H₂ production from the Co(III)H as has been postulated for a more elaborately substituted Co chlorin.¹² That the catalysis occurs at the first reduction wave rather than at a more negative potential indicates that the second electron transfer occurs at a potential positive of the first ($E_2^0 > E_1^0$).⁴⁵ Thus, the catalysis appears to occur at the Co(II/I) wave, as the second CV wave for the second reduction shifts inside (more positive) the first reduction wave upon protonation following the first reduction process. These results are consistent with the chlorin exhibiting increased basicity as compared to porphyrins, which exhibit HER upon a second reduction that is more negative than the first reduction ($E_1^0 > E_2^0$).⁴⁶ Moreover, **1-Co** is also distinct from Nature's cobalt tetrapyrrole, cobalamin, which is reduced at too positive a potential for HER, with no further reductions observed, thus resulting in cobalamin being incapable of HER from weak acids.⁴⁹ We also note that ligand involvement in the delivery of protons to the metal center to either form or protonate a metal hydride has been proposed in mechanisms for HER catalysts possessing pendant amines,⁴⁷ pendant carboxylic acids,^{46,48} or even carbon atoms in aromatic ligands.⁴⁹ Although protonation of the *meso* or β carbon atoms of macrocyclic ligands has been proposed,⁵⁰ our present studies of **1-Co** have uncovered no evidence for the chlorin ligand directly participating in proton transfer steps.

The plateau current also gives direct access to the apparent rate constant of the catalytic reaction.⁴² In the context of an ECEC mechanism, Savéant and Artero have shown that the rate constants k_1 and k_2 of the first and second chemical steps (proton transfers in Scheme 1) may be deduced from the plateau current (i_{pl}), which is normalized by the current of the one-electron wave in the absence of acid, i_p^0 , and the half-wave potential ($E_{1/2}$), according to the following,⁴³

$$\frac{i_{pl}}{i_p^0} = 4.48 \sqrt{\frac{RT}{F\nu} \frac{\sqrt{k_1 k_2 [AH]}}{\sqrt{k_1} + \sqrt{k_2}}} \quad (1)$$

$$E_{1/2} = E_1^0 + \frac{RT}{F} \ln \left(1 + \sqrt{\frac{k_1}{k_2}} \right) \quad (2)$$

where ν is the scan rate and $E_1^0 = E_{1-}^0 = -1.401$ V vs. Fc⁺/Fc in this case. The values of the two rate constants can be determined from Eqs. (1) and (2) by parametrically fitting Eq. (1) to the experimental data shown in Figure

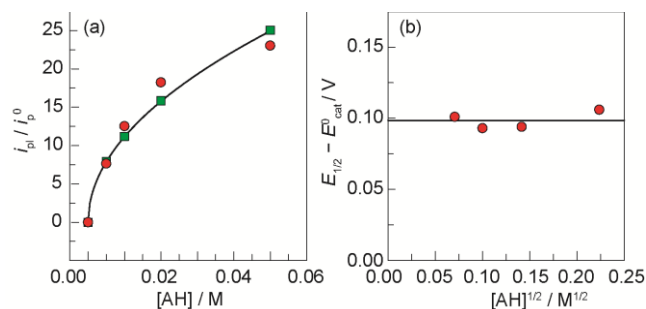


Figure 10. Analysis of the data in Figure 9a: (a) Variation of the normalized plateau current (●) with the acid concentration and least-squares fitting (—) of the experimental data to Eq. (1) and expected normalized plateau currents (■) using Eq. (1) and $k_1 = 5.7 \times 10^6 \text{ M}^{-1} \text{ s}^{-1}$ and $k_2 = 2.6 \times 10^3 \text{ M}^{-1} \text{ s}^{-1}$. (b) The half-wave potential (●) with the square root of the acid concentration; average value (—).

10a and Eq. (2) to the average half-wave potential of the data shown in Figure 10b. The details of the fitting procedure are described in Section F of the Supporting Information to furnish the rate constants $k_1 = 5.7 \times 10^6 \text{ M}^{-1} \text{ s}^{-1}$ and $k_2 = 2.6 \times 10^3 \text{ M}^{-1} \text{ s}^{-1}$. Using these calculated rate constants, values of the normalized plateau current from Eq. (1) agree well with the experimental data (green squares in Figure 10a).

The HER catalytic activity of **1-Co** can be benchmarked by the methods of Savéant and Artero^{42,43} to furnish “catalytic Tafel plots”, which represent the evolution of the turnover frequency (TOF) as a function of the overpotential (η) of the catalytic reaction. This approach is independent of experimental factors, such as cell configuration, and includes in the calculation of the TOF only the amount of active catalyst present in the reaction diffusion layer, thereby providing a rational method of benchmarking intrinsic catalytic activity. An efficient catalyst will exhibit a high turnover frequency at low overpotential and consequently is situated in the top left corner of Figure 11. The TOF as related to HER is given by,^{42,43}

$$TOF = \frac{TOF_{max}}{1 + \exp \left[\frac{F}{RT} (E_{H^+/H_2}^0 - E_{1/2}) \right] \exp \left(-\frac{F}{RT} \eta \right)} \quad (3)$$

$$TOF_{max} = \frac{k_1 k_2}{k_1 + k_2} [AH] \quad (4)$$

where TOF_{max} is the maximal value of the TOF. From this equation, the previously determined values of k_1 and k_2 yield TOF_{max} for a given concentration of acid. The “catalytic Tafel plots” (Figure 11) are constructed by inputting a concentration of $[AH] = 1$ M for each catalyst into Eq. (4). The TOF scales with overpotential, η , as described by Eq. (3). The thermodynamic standard potential for hydrogen generation, E_{H^+/H_2}^0 , from TFA at a concentration of 1 M is calculated to be -0.62 V vs. Fc⁺/Fc using the method established by Fourmond et al.⁵¹ This value of E_{H^+/H_2}^0 takes into account the effect of

homoconjugation, which is the association of an acid with its conjugate base via hydrogen bonding. The equilibrium constant for homoconjugation of TFA in CH₃CN is $7.9 \times 10^3 \text{ M}^{-1}$.³⁹ $E_{1/2}$ is determined from the CVs in Figure 9a to be -1.302 V vs. Fc⁺/Fc. From these values, the plot of TOF vs. η for HER for **1-Co** can be constructed, and is presented in Figure 11 together with the activity curves of other reported HER catalysts,^{52–56} including an Fe porphyrin.⁵² **1-Co** is a superior HER catalyst as compared to porphyrins at all η , and especially in the low η region. Inasmuch as energy conversion cycles seek to perform catalysis at low overpotential, the connection of η to TOF is the critical metric in catalyst design.

CONCLUSION

Insertion of a Co(II) ion into a sparsely substituted chlorin (**1-Co**) induces significant out-of-plane distortion of the macrocycle. Structural comparisons between metal-free and Co chlorins reveal a constriction of the macrocycle core and a possible mitigation of the destabilizing effect of anti-aromaticity in the 20 π -electron conjugated pathway due to the presence of the Co(II) ion. EPR, electronic absorption and time-resolved absorption spectra are consistent with the presence of an open-shell, $S = 1/2$, metal center residing within the chlorin ligand environment. The electrochemistry of **1-Co** speaks to significant coupling of the Co d-orbitals with those of the electron-rich chlorin macrocycle. Efforts to perform the electrocatalytic oxygen reduction reaction (ORR) with **1-Co** revealed that the Co chlorin is unstable to the combined presence of oxygen and acid, which are requisite for ORR chemistry. However, the Co chlorin decomposition product formed under such conditions is competent for ORR. **1-Co** is an authentic electrocatalyst for the hydrogen evolution reaction (HER), with the caveat that acids that are too strong will cause demetalation. With weaker acids such as trifluoroacetic acid, **1-Co** performs HER via a proposed mechanism involving the protonation of Co(II) hydride to afford H₂. The ability of the Co chlorin to perform HER via an intermediate that is reduced at a standard potential positive of that of the first reduction of the complex is in contradistinction to Co porphyrins, which catalyze HER from acids, regardless of strength, at potentials well negative of the first reduction (therefore leading to higher overpotentials).⁴⁶ The origin for this disparate behavior does not arise from the redox properties of the macrocycle, as **1-Co** and Co tetraphenylporphyrin undergo multiple reduction and oxidations in similar potential ranges.³⁴ The increased activity of **1-Co** as compared to porphyrins appears to be derived from the increased electron density of the chlorin macrocycle, thus leading to a more basic Co(I) metal center, in turn promoting hydride formation and subsequent reduction to Co(II) hydride. The importance of cobalt basicity on such a Co(I) \rightarrow Co(III)H \rightarrow Co(II)H reaction sequence for HER has been theoretically established.⁵⁷ Examination of

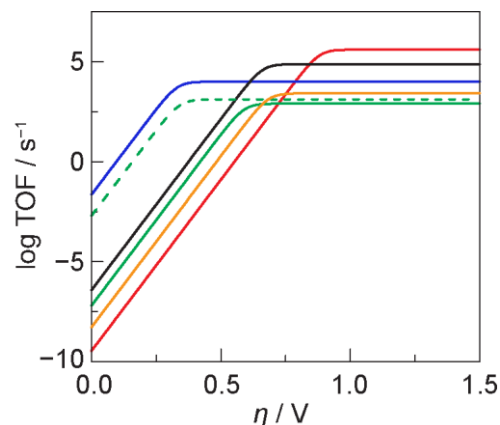


Figure 11. Catalytic Tafel plots for the different electrocatalysts listed in Table 1 of ref. 43 and for **1-Co** based on the data in Table 1: FeTPP in DMF and Et₃NH⁺ (—); Co(dmgh)₂py in DMF and Et₃NH⁺ (—); [Ni(P₂PhNPh)₂]²⁺ in CH₃CN and DMFH⁺ (—); [Ni(P₂PhN₂C₆H₄X)₂]²⁺ in CH₃CN and TfOH with X = H (—) and in CH₃CN and DMFH⁺ with X = CH₂P(O)(OEt)₂ (—); **1-Co** in CH₃CN and TFA (—).

the electrochemical kinetics of **1-Co** has revealed HER to proceed by an ECEC mechanism, and allowed us to obtain the key chemical rate constants (k_1 and k_2 in Scheme 1) of the ECEC catalytic cycle. From these rate constants, the catalytic activity as related by the TOF for HER has been determined. Upon benchmarking the catalytic activity of molecular HER catalysts, we find that at low overpotentials the Co chlorin **1-Co** exhibits superior HER activity as compared to its porphyrin congeners.

ASSOCIATED CONTENT

Supporting Information

Electronic Supplementary Information (ESI) available: materials, experimental methods, description of data analysis and instrumentation, X-ray crystallographic information, mass spectrometry, gas chromatography, and additional UV-vis and cyclic voltammetry data. See DOI: XXXXXXXX

AUTHOR INFORMATION

Corresponding Authors

* E-mail: jlindsey@ncsu.edu (JSL)

* E-mail: dnocera@fas.harvard.edu (DGN)

Author Contributions

‡ These authors contributed equally to this work

ACKNOWLEDGMENTS

We thank Seung Jun Hwang for assistance with gas chromatography. This material is based upon work supported under the Solar Photochemistry Program of the Chemical Sciences, Geosciences and Biosciences Division, Office of Basic Energy Sciences of the U. S. Department of Energy (DGN) and by a grant DE-FG02-05ER15651 from the Chemical Sciences, Geosciences and Biosciences Division, Office of Basic Energy Sciences, of the U. S. Department of Energy (JSL).

REFERENCES

- (1) Taniguchi, M.; Mass, O.; Boyle, P. D.; Tang, Q.; Diers, J. R.; Bocian, D. F.; Holten, D.; Lindsey, J. S. *J. Mol. Struct.* **2010**, *979*, 27–45.
- (2) Lemon, C. L.; Dogutan, D. K.; Nocera, D. G. In *Handbook of Porphyrin Chemistry*; Kadish, K. M., Smith, K. M., Guillard, R., Eds; Academic Press: Amsterdam, **2012**, Vol. 21, Ch. 99, p. 144.
- (3) Rosenthal, J.; Nocera, D. G. *Acc. Chem. Res.* **2007**, *40*, 543–553.
- (4) Collman, J. P.; Wagenknecht, P. S.; Hutchison, J. E. *Angew. Chem., Int. Ed.* **1994**, *33*, 1537–1554.
- (5) Brothers, P. J.; Collman, J. P. *Acc. Chem. Res.* **1986**, *19*, 209–215.
- (6) Chang, D.; Malinski, T.; Ulman, A.; Kadish, K. M. *Inorg. Chem.* **1984**, *23*, 817–824.
- (7) Stolzenberg, A. M.; Stershic, M. T. *Inorg. Chem.* **1987**, *26*, 1970–1977.
- (8) Stolzenberg, A. M.; Strauss, S. H.; Holm, R. H. *J. Am. Chem. Soc.* **1981**, *103*, 4763–4778.
- (9) Fujita, E.; Fajer, J. *J. Am. Chem. Soc.* **1983**, *105*, 6743–6745.
- (10) Mase, K.; Ohkubo, K.; Fukuzumi, S. *J. Am. Chem. Soc.* **2013**, *135*, 2800–2808.
- (11) Mase, K.; Ohkubo, K.; Fukuzumi, S. *Inorg. Chem.* **2015**, *54*, 1808–1815.
- (12) Aoi, S.; Mase, K.; Ohkubo, K.; Fukuzumi, S. *Chem. Commun.* **2015**, *51*, 15145–15148.
- (13) Lindsey, J. S. *Chem. Rev.* **2015**, *115*, 6534–6620.
- (14) Taniguchi, M.; Ra, D.; Mo, G.; Balasubramanian, T.; Lindsey, J. S. *J. Org. Chem.* **2001**, *66*, 7342–7354.
- (15) Gallucci, J. P.; Sweptson, P. N.; Ibers, J. A. *Acta Cryst.* **1982**, *B38*, 2134–2139.
- (16) Taniguchi, M.; Lindsey, J. S. *Chem. Rev.* **2017**, *117*, 344–535.
- (17) Taniguchi, M.; Kim, H.-J.; Ra, D.; Schwartz, J. K.; Kirmaier, C.; Hindin, E.; Diers, J. R.; Prathapan, S.; Bocian, D. F.; Holten, D.; Lindsey, S. J. *J. Org. Chem.* **2002**, *67*, 7329–7342.
- (18) Alben, J. O. *The Porphyrins*; Dolphin D. Eds; Academic Press: New York, **1978**, Vol. III, Physical Chemistry Part A Ch. 7, p 323.
- (19) Collman, J. P.; Berg, K. E.; Sunderland, C. J.; Aukauloo, A.; Vance, M. A.; Solomon, E. I. *Inorg. Chem.* **2002**, *41*, 6583–6596.
- (20) Honda, T.; Kojima, T.; Fukuzumi, S. *J. Am. Chem. Soc.* **2012**, *134*, 4196–4206.
- (21) Clegg W. Ed. *Crystal Structure Analysis: Principles and Practice*; 2nd Ed. Oxford University Press: New York, 2009.
- (22) Gouterman, M. *J. Mol. Spectrosc.* **1961**, *6*, 138–163.
- (23) Kee, H. L.; Kirmaier, C.; Tang, Q.; Diers, J. R.; Muthiah, C.; Taniguchi, M.; Laha, J. K.; Ptaszek, M.; Lindsey, J. S.; Bocian, D. F.; Holten, D. *Photochem. Photobiol.* **2007**, *83*, 1110–1124.
- (24) Kee, H. L.; Kirmaier, C.; Tang, Q.; Diers, J. R.; Muthiah, C.; Taniguchi, M.; Laha, J. K.; Ptaszek, M.; Lindsey, J. S.; Bocian, D. F.; Holten, D. *Photochem. Photobiol.* **2007**, *83*, 1125–1143.
- (25) Aravindu, K.; Kim, H.-J.; Taniguchi, M.; Dilbeck, P. L.; Diers, J. R.; Bocian, D. F.; Holten, D.; Lindsey, J. S. *Photochem. Photobiol. Sci.* **2013**, *12*, 2089–2109.
- (26) Tait, C. D.; Holten, D.; Gouterman, M. *Chem. Phys. Lett.* **1983**, *100*, 268–272.
- (27) Yu, H.; Baskin, J.; Steiger, B.; Wan, C.; Anson, F.; Zewail, A. *Chem. Phys. Lett.* **1998**, *293*, 1–8.
- (28) Fukuzumi S.; Ohkubo, K.; Imahori, H.; Shao, J.; Ou, Z.; Zheng, G.; Chen, Y. Pandey, R. K.; Fujitsuka, M.; Ito, O.; Kadish, K. M. *J. Am. Chem. Soc.* **2001**, *123*, 10676–10683.
- (29) Stolzenberg, A. M.; Spreer, L. O.; Holm, R. H. *J. Am. Chem. Soc.* **1980**, *102*, 364–370.
- (30) Kadish, K. M.; Royal, G.; Van Caemelbecke, E.; Gueletti, L. In *The Porphyrin Handbook*. Kadish, K. M.; Smith, K. M.; Guillard, R., Eds. Academic Press: San Diego, CA, 2000; Vol. 9, p. 14.
- (31) Tait, C. D.; Holten, D.; Gouterman, M. *J. Am. Chem. Soc.* **1984**, *106*, 6653–6659.
- (32) Dolphin, D.; Muljiani, Z.; Rousseau, K.; Borg, D. C.; Fajer, J.; Felton, R. H. *Ann. N. Y. Acad. Sci.* **1973**, *206*, 177–200.
- (33) Kobayashi, H.; Kaizu, Y.; Hara, T. *Bull. Chem. Soc. Jpn.* **1972**, *45*, 2148–2155.
- (34) D'Souza, F.; Villard, A.; Van Caemelbecke, E.; Franzen, M.; Boschi, T.; Tagliatesta, P.; Kadish, K. M. *Inorg. Chem.* **1993**, *32*, 4042–4048.
- (35) Gouterman, M. In *The Porphyrins* **1978**, 3. Dolphin D. Eds; Academic Press: New York, **1978**, Vol. III, Physical Chemistry Part A, p. 1.
- (36) Whitlock, H. W.; Bower, B. K. *Tetrahedron Lett.* **1965**, 4827–4831.
- (37) Doppelt, P.; Fischer, J.; Weiss, R. *Inorg. Chem.* **1984**, *23*, 2958–2962.
- (38) Lemon, C. M.; Huynh, M.; Maher, A. G.; Anderson, B. L.; Bloch, E. D.; Powers, D. C.; Nocera, D. G. *Angew. Chem., Int. Ed.* **2016**, *55*, 2176–2180.
- (39) Izutsu, K. *Acid-Base Dissociation Constants in Dipolar Aprotic Solvents*; Blackwell: Boston, 1990.
- (40) Argüello, J. E.; Costentin, C.; Griveau, S.; Savéant, J.-M. *J. Am. Chem. Soc.* **2005**, *127*, 5049–5055.
- (41) Costentin, C.; Passard, G.; Robert, M.; Savéant, J.-M. *Chem. Sci.* **2013**, *4* (2), 819–823.
- (42) Costentin, C.; Savéant, J.-M. *ChemElectroChem.* **2014**, *1*, 1226–1236.
- (43) Artero, V.; Savéant, J.-M. *Energy Environ. Sci.* **2014**, *7*, 3808–3814.
- (44) Savéant, J.-M. *Elements of Molecular and Biomolecular Electrochemistry: an Electrochemical Approach to Electron Transfer Chemistry*; John Wiley: Hoboken, NJ, **2006**, p. 106.
- (45) Costentin, C.; Dridi, H.; Savéant, J.-M. *J. Am. Chem. Soc.* **2014**, *136*, 13727–13734.
- (46) Lee, C. H.; Dogutan, D. K.; Nocera, D. G. *J. Am. Chem. Soc.* **2011**, *133*, 8775–8777.
- (47) O'Hagan, M.; Shaw, W. J.; Raugel, S.; Chen, S.; Yang, J. Y.; Kilgore, U. J.; DuBois, D. L.; Bullock, R. M. *J. Am. Chem. Soc.* **2011**, *133*, 14301–14312.
- (48) Bediako, D. K.; Solis, B. H.; Dogutan, D. K.; Roubelakis, M. M.; Maher, A. G.; Lee, C. H.; Chambers, M. B.; Hammes-Schiffer, S.; Nocera, D. G. *Proc. Natl. Acad. Sci. U.S.A.* **2014**, *111*, 15001–15006.
- (49) Quintana, L. M. A.; Johnson, S. I.; Corona, S. L.; Villatoro, W.; Goddard, W. A.; Takase, M. K.; VanderVelde, D. G.; Winkler, J. R.; Gray, H. B.; Blakemore, J. D. *Proc. Natl. Acad. Sci. U.S.A.* **2016**, *113*, 6409–6414.

1 (50) Solis, B. H. ; Maher, A. G. ; Dogutan, D. K. ; Nocera, D.
2 G.; Hammes-Schiffer, S. *Proc. Natl. Acad. Sci. U.S.A.* **2016**,
3 *113*, 485-492.

4 (51) Fourmond, V.; Jacques, P.-A.; Fontecave, M.; Artero, V.
5 *Inorg. Chem.* **2010**, *49*, 10338-10347.

6 (52) Bhugun, I.; Lexa, D.; Savéant, J.-M. *J. Am. Chem. Soc.*
7 **1996**, *118*, 3982-3983.

8 (53) Razavet, M.; Artero, V.; Fontecave, M. *Inorg. Chem.*
9 **2005**, *44*, 4786-4795.

10 (54) Helm, M. L.; Stewart, M. P.; Bullock, R. M.; DuBois, M.
11 R.; DuBois, D. L. *Science* **2011**, *333*, 863-866.

12 (55) Kilgore, U. J.; Roberts, J. A. S.; Pool, D. H.; Appel, A.
13 M.; Stewart, M. P.; DuBois, M. R.; Dougherty, W. G.; Kassel,
14 W. S.; Bullock, R. M.; DuBois, D. L. *J. Am. Chem. Soc.* **2011**,
15 *133*, 5861-5872.

16 (56) Wilson, A. D.; Newell, R. H.; McNevin, M. J.;
17 Muckerman, J. T.; Rakowski DuBois, M.; DuBois, D. L. *J. Am.*
18 *Chem. Soc.* **2006**, *128*, 358-366.

19 (57) Muckerman, J. T.; Fujita, E. *Chem. Commun.* **2011**, *47*,
20 12456-12458.

21
22
23
24
25
26
27
28
29
30
31
32
33
34
35
36
37
38
39
40
41
42
43
44
45
46
47
48
49
50
51
52
53
54
55
56
57
58
59
60

TOC

